

Research paper

Performance of a low power Hall effect thruster with several gaseous propellants

Thomas F. Munro-O'Brien ^{*1}, Charles N. Ryan ²*University of Southampton, Highfield Campus, Southampton, SO17 1BJ, United Kingdom*

ARTICLE INFO

Keywords:

Hall effect thruster
Alternative propellants
Krypton
Argon
Scaling
Nitrogen

ABSTRACT

There is a growing need to consider alternative propellants for operation in Hall thrusters, away from the conventional legacy of using xenon. This is particularly the case for small Hall thrusters; which are growing exponentially in their use, whilst needing to be operational on inexpensive propellants. Alternative propellants include condensable propellants (i.e., zinc and iodine), or other gaseous propellants (krypton, argon, and nitrogen (N_2)) - which are the focus here. A low power (nominally 100 W) miniature Hall thruster has been designed and manufactured based upon standard scaling laws, with specific considerations for operation with the use of alternative gaseous propellants, and with an attempted novel field topology. The thruster, designated the HEKT-100, was designed to be a low power magnetically shielded thruster to operate on krypton, however the level of shielding present is unknown or tested. Here the thruster has subsequently been operated on xenon, krypton, argon, and diatomic nitrogen successfully, with an unstable operation with neon. The thruster is operated at discharge powers of between 30–810 W. Using a pendulum thrust balance, the thruster performance was measured across a wide range of flow rates, magnetic field strengths, and anode discharge voltages. The performance measured for xenon, krypton, argon, and diatomic nitrogen respectively was, peak thrusts of 12.6 mN, 6.9 mN, 6.6 mN and 5.7 mN, anode efficiencies up to 26.3%, 15.2%, 9.6% and 5.4%, and specific impulses up to 2160 s, 1730 s, 1390 s, and 1000 s. This dataset and the following analysis provides one of the few times a comprehensive selection of alternative gaseous propellants have been tested within the same thruster and compared directly with unchanged geometry or set-up.

1. Introduction

In recent years the applications of satellites have rapidly increased. Be it micro to nano class satellites or precise formation flying low Earth orbit constellations, satellites are becoming a more federated system with single missions being carried out by several satellites [1]. Satellites today are moving from massive and expensive platforms in geostationary orbit towards smaller, single purpose, bespoke satellites for specific low Earth orbit applications [2]. A class of satellites showing large growth due to economic robustness and versatility of the platform is the micro and nano-class of satellites [3]. These trends are creating new and unique demands of the propulsion systems. This has motivated interest and demand on research in Hall effect thrusters due to the possibility that they can fulfil these requirements of lower operational powers without sacrificing the benefits of an electric propulsion system. The addition of a low power, long life Hall effect thruster has been identified as an enabling technology for low-mass spacecraft on the order of 100–300 kg [4].

A Hall effect thruster (HET) is a type of electric propulsion (EP) that utilises both magneto-static and electrostatic fields to accelerate ions to produce thrust [5]. This type of thruster is primarily attractive for large ΔV missions due to the high specific impulse, whilst also offering a higher thrust to power ratio than comparative EP systems [6]. These advantages of the platform have driven HETs to become the most utilised form of propulsion in space today [7,8].

Hall effect thrusters have been utilised in space for half a century as of 2022, with the first use of the HET in space being the former USSR Meteor satellite launched in 1972 [3,9,10]. When compared to a gridded ion thruster (GIT), HETs offer a unique set of advantages with higher thrust to power ratios as well as higher achievable power densities for a given physical envelope with regards to scaling. However, the primary attraction of HETs systems over GITs is the simple thruster architecture, making HETs a relatively lower cost and more reliable propulsion system. Historically, research and interest in HETs has been focused around the 1 kW power regime, but with the recent

^{*} Corresponding author.

E-mail address: tfmo1e17@soton.ac.uk (T.F. Munro-O'Brien).

¹ Doctoral candidate.

² Associate professor.

expansion of the micro and nano satellite markets this has increased the development of smaller, lower power Hall thruster platforms.

The majority of Hall effect thrusters with flight heritage operate at discharge powers in excess of several kilowatts, with only recent research and commercial developments targeting scaling to lower power regimes [2,11–13]. The current trend is away from well tested medium sized satellites and towards low cost, low power, and more agile solutions for low Earth applications. One such example of these increasing demands for small satellites is telecommunication mega constellations. The “Starlink” constellation of a planned 4025 satellites is utilising HETs for orbit raising and station keeping in low earth orbit [1, 7]. For many such small satellite platforms in low earth orbit constellation and other precision flying applications, a large range of requirements are put upon the propulsion subsystem, due to the high drag environment and a requirement to minimise the propellant mass fraction [1]. However, HETs are ill-suited for high precision formation flying, e.g., multi-satellite interferometry payloads but, due to their high thrust, are good for drag compensation, orbit transfers, as well as collision avoidance manoeuvres when compared to other electro-static propulsion.

New Hall thrusters for operation at low power levels need to be carefully designed as several aspects of the operation are altered in miniaturisation. To enable thruster scaling, several studies have suggested analytical and empirical methods of scaling Hall effect thrusters to a wide range of powers that provide rapid sizing estimates [13–15]. Offering a primarily empirical method these scaling relationships show good agreement on results at scaling to sub-kilowatt powers, although are lacking in their high-fidelity agreement to experimental results. This results from the plasma interactions with the channel walls becoming the dominating power loss mechanisms and the reduced plasma volume at low powers. As these effects are exacerbated within low power Hall thrusters, utilising a database of majority high power HETs for scaling to the sub-kilowatt level will inherently neglect these effects.

Xenon is an excellent propellant for electric propulsion due to being inert, its low ionisation energy, and a high atomic mass. However, as the primary production of xenon is as a by-product of other industries, this in combination with a low natural abundance results in high cost as well as a high level of volatility to the supply [16]. The global production of xenon is approximately 53,000 kg a year, such that any mission requiring several tons of propellant would undoubtedly have a large impact on the cost and global supply of xenon [17]. Such a quantity of propellant is not absurd, with some Mars-Earth mission analysis predicting the use of 20,000–23,000 kg of xenon for a single round trip, or the planned Lunar Gateway space station requiring 2,750 kg of xenon for the yearlong orbit transfer and 2–5 kg of xenon a year for station keeping thereafter [18–20]. The prohibitive cost and volatility of the xenon supply will only worsen as more space missions utilise electric propulsion.

Krypton has been suggested as an alternative to xenon due to a significantly lower cost per kg; as of late 2022 due to global economic downturn and greater turmoil within global supply chains, xenon prices were approximately 7.5–10 k€/kg. The move to krypton also offers a higher theoretically achievable specific impulse for a constant discharge voltage, although at a cost to overall efficiency [21]. These losses could perhaps be minimised through the use of more novel or optimised field and channel topologies, although the same efficiency for xenon and krypton from the same Hall thruster cannot be achieved due to the lower ionisation energy and larger cross-sectional area of ionisation of xenon. Such that, xenon will have a greater mass utilisation than krypton if the geometry is not optimised [22].

Due to the growing need to find an alternative to xenon within the industry as well as trends towards reducing costs for manufacturing and operating satellites, a wide variety of propellants are being investigated. Condensable propellants have been proposed as alternatives to xenon as many of these alternatives can offer similar thrust capabilities and additional propellant storage densities [23–27]. However, the change

from gaseous to condensable propellants come with additional system complexities that have yet to be fully resolved. As a result of the highly risk-adverse nature of satellite design, gaseous alternatives have had much greater success in development and research interest.

Krypton has been investigated as an alternative to xenon for almost two decades, with progress towards higher efficiencies in large high-power thrusters but with less focus on low power systems [21,28–31]. Several other inert gases may be viable alternatives with similar operation and performance to krypton with further potential cost savings. Moreover, if these alternatives are lower in atomic mass, such as argon, additional specific impulse could be extracted from the propellant for equivalent discharge voltages.

Prior work has identified that krypton operating in the same thruster has a lower anode efficiency than xenon [22,31,32]. This has been found to be predominately due to a decrease in mass utilisation and current utilisation efficiencies for krypton operation [21]. Novel field topologies such as magnetic shielding (MS) have been suggested as a method to make alternative, harder to ionise, propellants more viable. Due to the nature of MS topologies, they generally experience higher plasma temperatures in the ionisation region than that of an unshielded configuration [21,33]. These higher plasma temperatures could lead to increased ionisation rates of the propellant; providing a more desirable plasma environment due to the higher energy electrons, although the higher plasma temperatures will result in greater radiative losses.

Further research into magnetically shielded thrusters has been undertaken in recent years [12,21,34]. Whilst the majority of success of magnetically shielded thrusters has been in the high-power regimes, there has been a question of applying this life extending technique to smaller sub-kilowatt thrusters [35–38].

Here a low power miniature Hall thruster has been successfully operated without redesign, and without alteration to propellant delivery system with several easily obtainable and storable gaseous propellants. This has been done with the purpose to gain insight into the operation and performance of the thruster across a wide range of different propellants, more than has been tested previously in the same thruster.

2. Hall Thruster design

The Hall effect thruster designed and tested at the University of Southampton has been designated the Hall Effect Krypton Thruster 100 Watts (HEKT-100). Its initial design and operation on krypton has been described elsewhere; here the testing of the thruster is extended to include additional alternative propellants and further testing on krypton [36]. However, although the design was initially intended to operate as a magnetically shielded Hall thruster, it is important to note that a validity and effectiveness of this novel field topology is untested and unknown. Moreover, from measurements of the field it is deemed unlikely to be a MS topology.

2.1. Design method

The HEKT-100 Hall thruster was designed and scaled to the target of 100 Watts via the use of database scaling as outlined by Dannenmayer et al. as well as use of a specifically sub-kilowatt database of HETs from a similar scaling method as described by Lee et al. [15,36,39].

Both methods used are semi-empirical and share similarities, with both derived from correlations present in databases of thrusters with flight heritage, in conjunction with simplified plasma properties and thruster performance equations. Dannenmayer [15] uses a database of 33 thrusters ranging in power of 10 W–50 kW, whilst Lee [39] used 17 exclusively sub-kW thrusters with slight variations on the scaling equations derived. Both methods are based upon establishing a group of equations that allow a complete thruster channel geometry to be obtained from an input anode power and voltage.

These scaling methods require several assumptions and stipulations. Firstly, the anode mass flow rate is chosen to meet an optimal neutral

number density within the channel. From literature [5,15], this has been found empirically to be $n_{n,c} \approx 1.2 \times 10^{19} \text{ m}^{-3}$, whilst electron number density was found to be $n_e \approx 0.1 \times n_n = 1.2 \times 10^{18} \text{ m}^{-3}$. This ensures a sufficient rate of ionisation and optimal thermal effects, as found by Dannenmayer et al. [40]. Secondly, the electron temperature is also an important parameter for characterising the plasma potential and bulk electron behaviour within analysis. Within both scaling methods considered here, this value was to be preserved through scaling [15,39].

It is important to note that the critical number density used throughout this paper is a semi-empirical value found from the operation of several high-power flight-tested Hall thrusters [5,15]. This value has since been used for scaling approximations for thrusters of all sizes operating on xenon [5,41]. However, no critical value has been determined for alternative propellants. J. Linnell et al. found an optimised number density for krypton operating in the NASA-173Mv1 Hall thruster of $n_n \approx 0.8 \times 10^{19}$ at 500 V anode discharge [42]. However, other testing showed no significant differences in efficiencies between xenon and krypton at identical neutral number densities in the NASA-457M thruster [43]. These studies were done with high power xenon designed thrusters adding additional uncertainty to the application of these findings to alternative propellant intended thruster designing. Due to the lack of a clear alternative, the following analysis will use the critical number density as reported by Dannenmayer et al. for all propellants considered [40].

An estimation of the bulk electron temperature is [15],

$$T_e \approx 0.12U_d \quad (1)$$

where U_d is the anode discharge voltage. However, whilst Eq. (1) has been confirmed for standard HETs operating on xenon, this will likely underestimate the electron temperature for novel field topologies such as magnetic shielding or operation with alternative propellants. Non-invasive incoherent Thompson-scattering measurements of electron temperatures have been undertaken by B. Vincent et al. within the low power ISCT200 operating on xenon, with and without a magnetically shielded field topology. This change in field configuration suggested an increase of 2–3 times greater the electron temperature, than is predicted by Eq. (1), at the exit plane of the thruster [33]. Additionally, another study by R. Hofer et al. utilising invasive Langmuir probe measurements of electron temperature within the H6 6 kW Hall thruster showed an increase in electron temperature. However, the electron temperature increase was at a significantly reduced magnitude than found by B. Vincent, an approximate increase of 8–10 eV [44]. Whilst only two examples, these show that there is an increase in electron temperature from a standard Hall thruster configuration to a magnetically shielded topology. Moreover, there is a large variation within the electron temperature measurements for MS Hall thrusters operating on xenon further casting doubt on the extension of Eq. (1) for use with alternative propellants.

Furthermore, it is also assumed that the neutral propellant is released at a temperature equal to the assumed anode temperature of 800 K, however noting within literature this applied value has been varied between 800–1300 K [15,45,46]. For calculations completed here a neutral propellant temperature of 800 K was used, although this range has a non-negligible effect on the ionisation mean free path, the distance a neutral atom will travel before the probability of an ionising collision having occurred is approximately unity. This is a result of the assumption that the neutral propellant will travel with a constant thermal velocity throughout the channel length, L , and therefore is directly linked to the transit time for the propellant within the thruster. For example, the neutral velocity can be assumed as the 3-dimensional thermal velocity at a temperature of the assumed anode temperature described as,

$$u_n = \sqrt{\frac{8K_B T_a}{\pi m_n}} \quad (2)$$

where T_a is the assumed anode temperature, m_n is the neutral mass, and K_B is the Boltzmann constant. Using Eq. (2) for xenon at 800 K and 1300 K gives a velocity of 360 ms⁻¹ and 460 ms⁻¹, respectively. However, these kinds of approximations cannot be entirely avoided in broad scaling methods.

This discrepancy in thermal neutral velocity will be magnified when considering the use of alternative propellants, due to the lower atomic mass of propellants considered. As the lighter neutral atoms will have a higher velocity for the same temperature, the magnitude of the variation of the neutral velocity for those propellants will be larger. The impact altering this assumption has on the scaling methods can be constructed to highlight the sensitivity of these methods to the underlying assumptions. By altering the neutral temperature for xenon, krypton and argon and calculating the impact that this has on the resulting scaled anode power for a constant desired thrust.

To calculate the variation of the anode power with different assumed neutral temperatures, the scaling relations as described by Dannenmayer et al. are applied [15]. For a constant target thrust the anode mass flow rate is taken as,

$$\dot{m}_n = \frac{T}{C_{T_1} \sqrt{U_d}} \quad (3)$$

where T is the target thrust of the design, C_{T_1} is a dimensional thrust scaling coefficient calculated from the database, and \dot{m}_n is the neutral mass flux to the anode. The anode mass flux can also be described in terms of neutral number density, propellant properties, and channel geometry such that,

$$\dot{m}_n = n_n \times m_n \times u_n \times A_c \quad (4)$$

where m_n is the neutral atomic mass and A_c is the cross-sectional area of the channel, and u_n is calculated using Eq. (2) where T_a is treated as a variable. As previously discussed in Section 2.1, the neutral number density is set to be equal to the critical neutral number density of $n_{n,c} \approx 1.2 \times 10^{19} \text{ m}^{-3}$. However, there is some uncertainty to the quality of this assumption, but due to the lack of any precedent on which to base an alternative estimate for each propellant, here it will be used unaltered. The cross-sectional channel area for an annular HET can be simply described as,

$$A_c = \frac{\pi}{4}(d_{outer}^2 - d_{inner}^2) = \pi h d \quad (5)$$

where h and d , are the channel width and mean channel diameter, respectively. The channel's geometric relationship between the mean channel diameter and channel width has been described within the scaling laws as;

$$h = C_{hd} d \quad (6)$$

where C_{hd} is the scaling coefficient relating channel width and mean channel diameter. Using Eqs. (5) and (6) the mass flow rate, Eq. (4) can now be described in terms of only mean channel diameter such that,

$$\dot{m}_n = n_n m_n u_n h d \pi = n_n u_n m_n \pi C_{hd} d^2 \quad (7)$$

From this the mean channel diameter can be described in terms of mass flow rate within the scaling relations as,

$$d = \sqrt{\frac{\dot{m}_n}{n_n u_n m_n \pi C_{hd}}} \quad (8)$$

The scaled power, in Watts, as described by Dannenmayer et al. [15] for a HET can be estimated via;

$$P = C_P U_d d^2 \quad (9)$$

where C_P is the power scaling coefficient. Combining Eq. (3)–(9) the resulting scaled anode power for a range of anode temperature is given by;

$$P(m_n, T_a) = \frac{C_P}{\pi C_{hd} C_{T_1}} \left[\frac{T \sqrt{U_d}}{n_{n,c} m_n u_n (m_n, T_a)} \right] \quad (10)$$

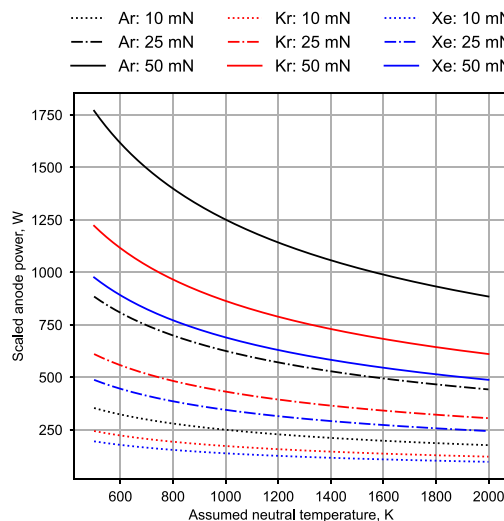


Fig. 1. A plot representing the sensitivity of scaling methods to the assumed neutral propellant temperature by showing the variation of scaled anode power for several design thrust levels and propellants. For all values shown the discharge is assumed 300 V and the neutral number density is set to the critical value.

This formulation is for a constant thrust, T , and discharge voltage, U_d . Each coefficient is formed from a database of existing thrusters and will vary depending on which database is used [15,39]. The value of the coefficients used are the same as were used to scale the HEKT-100 and are described elsewhere [36].

Eq. (10) shows the effect of altering the propellant comes from anode mass flow rate and neutral velocity being a function of propellant atomic mass. Fig. 1 is constructed from Eq. (10) by altering m_n for each propellant and the target thrust T , and then by varying the assumed anode temperature T_a all for the same discharge voltage of 300 V.

In Fig. 1 the resulting scaled HET anode discharge power for constant target thrust can be seen for three possible HET propellants at the three target input thrusts. It can be seen clearly that the effect of altering the assumed neutral temperature has a significantly magnified effect when considering argon when compared to the same target thrust of xenon. The effect of changing the assumed neutral temperature from 800 K to 1200 K, for the 50 mN case, causes a scaled anode power decrease of 142 W, 177 W, and 257 W for xenon, krypton, and argon respectively.

Comparing this result to a well-tested thruster with flight heritage, the BHT-1000 which operated on xenon, was able to produce approximately 50 mN at an anode power of 847 W. Using Eq. (10) and by assuming the thruster geometry follows the general scaling trends, this would suggest an approximate neutral temperature of 665 K; significantly lower than the scaling assumption of 800 K [47].

The scaling coefficients are not recalculated for each propellant as all thrusters used within the database operate exclusively on xenon. Moreover, this example is based upon a direct correlation between neutral number densities and channel geometry due to the assumption of constant “optimal” neutral number density. These both are potential oversights within the ability to scale thrusters and to the extent that this method can be extended to alternative propellants. However, the impact of the assumed anode temperature is clearly demonstrated within Fig. 1.

This method of drawing correlation from a database of thrusters with flight heritage can have some unintended outcomes. Dannenmayer et al. draw a direct relation between the mean channel diameter and the channel width, as can be seen in Eq. (6), with the strong relation suggested to be the result of photographic scaling from the SPT-100 by the designers of the HETs used within the database used [15]. However, there is some disagreement about this conclusion by Dannenmayer

Table 1

A comparison between the results of each scaling method utilised as well as the final chosen dimensions. The final selection varies somewhat from the scaled results due to a desire to increase the thruster volume to incorporate the magnetic circuit required for magnetic shielding.

	d, mm	h, mm	L, mm	\dot{m}_a , mg/s
Dannenmayer [15]	22.00	5.32	–	0.415
Lee [39]	22.95	5.50	–	0.380
Hybrid	22.20	5.68	–	0.412
Final design [36]	30.00	5.00	32.4	0.354

et al. Shagayda suggests there is a deeper, more fundamental reason for this apparent strong correlation; but neglects to comment directly on what this reason may be [14]. This suggestion comes from a series of thrusters developed at the Keldysh Research centre where a wide variety of channel widths and mean diameters were tested, resulting in the conclusion that the most optimal performance was found at the same ratio of channel width to mean channel diameter, although the data of these findings is not presented [14].

2.2. Resulting design

From several assumptions and methods as outlined within Section 2.1, a group of linear scaling equations are formed and used for HET design. Both Dannenmayer et al. and Lee et al. form different scaling equations and coefficients due to the use of differing methods and databases, however only the method as described by Dannenmayer et al. is discussed within Section 2.1. The resulting geometry from both methods is shown in Table 1, a third result is also shown as a hybrid method. This method results from utilising the equations as described by Dannenmayer and recalculating those coefficients using the database of sub-kilowatt thrusters provided by Lee et al. [15,39].

The chosen geometry is shown in Table 1, with the designed mean diameter chosen to be larger than the scaling results. This alteration was made to increase the internal volume of the thruster to allow for the required electromagnetic coils within the central core of the thruster body. These additional coils would enable finer control over the magnetic field topology as required for attempting a magnetically shielded topology. The mean channel diameter increase was accompanied by a reduction in the channel width, done to reduce the channel cross sectional area in an attempt to maintain the target anode power of 100 W, given that $P_{anode} \propto A_{channel}$ for a Hall thruster [15]. This can also be seen from Eq. (6) and (9) such that,

$$P = C_P U_d d^2 = C_P U_d d \frac{h}{C_{hd}} \propto h d \propto A_{Channel} \quad (11)$$

Even with this channel modification, the modified mean channel diameter and channel width resulted in a larger channel cross-sectional area than the original scaling. The new resulting scaled power can be obtained by using the same scaling equations. Reapplying the scaling relations with this modified channel, the new “designed” anode power is approximately 120 W at an anode voltage of 300 V. However, this choice to increase the mean diameter and decrease the channel width may have a significant impact on performance of the thruster. This change has increased the surface area to volume ratio of the channel annulus and further increase the losses associated with plasma-wall interactions. It can be seen that in a traditional Hall thruster annulus, the surface area to volume ratio of the plasma, if assumed to be approximately toroidal, can be taken as,

$$\frac{A_{surface}}{V_{plasma}} = \frac{4\pi^2 dh}{2\pi^2 dh^2} \propto \frac{1}{h} \quad (12)$$

where $A_{surface}$ is the plasma volumes surface area and V_{plasma} is the plasma volume. This is of interest as within a Hall thruster the volume of the plasma can be approximated as the source of the thrust whilst the surface area can be approximated as the source of significant wall

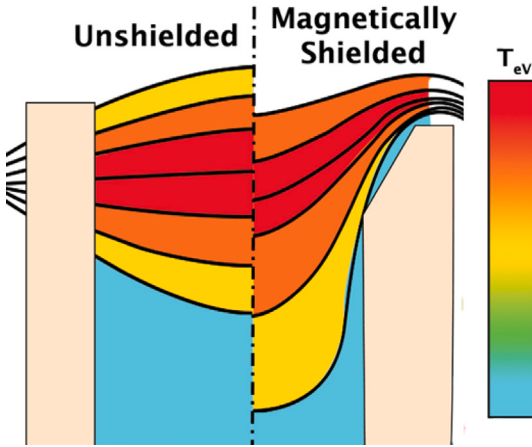


Fig. 2. A comparison between an unshielded (US) and a magnetically shielded (MS) configuration. Where T_{eV} is the electron temperature within the plasma.

losses, such that when the surface area to volume ratio is large the efficiency of the thruster will be reduced. As can be seen in Eq. (12) that this relationship is proportional to the inverse of the channel width, such that small channel widths will maximise these losses. Furthermore, it has also been seen in literature a large channel width increases propellant utilisation efficiency, in single stage xenon Hall thrusters [11]; hence the smaller channel width here may also be detrimental from a propellant utilisation perspective.

2.3. Magnetic shielding

Magnetic shielding (MS) is a widely accepted and utilised method of reducing or even eliminating the erosion of the Hall effect thruster's dielectric channel from impinging high energy ions. This Hall thruster design development has been a major advancement, given that the erosion of the dielectric channel has been the primary thruster lifetime-limiting factor, previously limiting its lifetime to much less than that of a gridded ion thruster. It has been shown that through the careful design of the magnetic field topology these erosion processes can be reduced or eliminated entirely [41,48,49].

Magnetic shielding is achieved by creating a magnetic field topology where the anode potential is maintained along the channel walls of the thruster, such that the electric field is orientated towards the channel centre line and away from the channel walls [41]. This maintaining of the high plasma potential in these regions prevents the ions impinging the channel wall from being significantly accelerated and as a result have lower kinetic energies on impact [41]. An illustration of the magnetic field lines and relative electron temperatures magnitudes present for an unshielded and a shielded topology can be seen in Fig. 2.

Magnetic shielding has been successfully implemented into several high power HETs, resulting in extended lifetimes and only a small reduction in performance [12,21,50]. The application of MS to low power Hall thrusters is though still an area of research, with smaller magnetically shielded thrusters maintaining similar beam divergence angle, but at a reduced thrust-to-power ratio, anode efficiencies and specific impulse than the high-power MS thrusters [3,37,38]. This has been attributed to several factors, such as a larger proportion of the plasma volume that is "sacrificed" as MS configurations there is a greater surface area to volume ratio within the plasma for the same channel width as the plasma does not directly interact with the walls as can be seen with Eq. (12). As low-power Hall thrusters have significantly smaller plasma volumes, reducing this further with an MS topology results in a larger percentage loss than with high power HETs.

Magnetically shielded topologies can have an additional benefit of decoupling the channel wall material and the plasma properties. It has

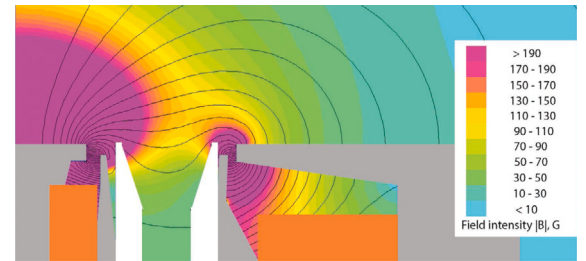


Fig. 3. Comparing the simulation of the thruster's magnetic field topology. The simulation was done in FEMM 4.2 and shows $|B|$ [36].

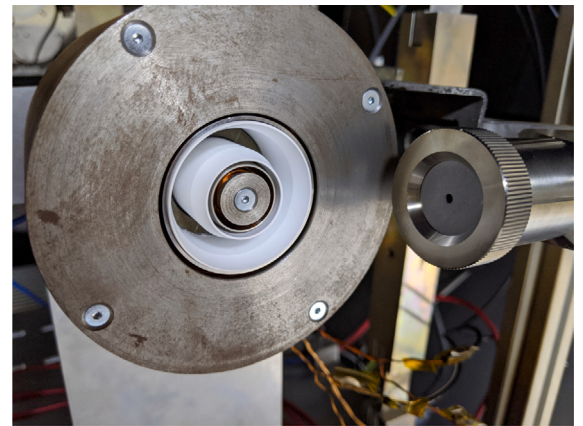


Fig. 4. The HEKT-100 mounted prior to testing in the large vacuum chamber at the University of Southampton.

been seen that changing the wall material can have a significant effect on performance and operation of a HET [51–53]. Due to the nature of MS topologies, there is a reduction in plasma interactions with the channel walls and as a result, alternative wall materials could be more readily considered [6].

The final field topology was modelled using the 2D axisymmetric modelling software "Finite Element Method Magnetics" (FEMM). The final topology can be seen in Fig. 3, where some of the field lines exhibit characteristic curving in a MS topology can be seen. However, this lacks sufficient magnitude to suggest a shielded topology and due to the lack of diagnostics the effectiveness of this magnetic topology at reducing erosion is unknown. However, the field is clearly not that of a traditional unshielded field topology and is still considered novel. The seen topology, in Fig. 3, has a peak field intensity outside the channel likely resulting in a larger than normal amount of plasma formation external to the thruster's channel and reducing performance. The manufactured thruster was measured to have a higher field strength than the modelling predicted. For all testing undertaken with the thruster the magnetic field was held constant by not altering the electromagnet coil current.

2.4. HEKT-100

The final manufactured thruster can be seen in Fig. 4 prior to testing. The scaling successfully assisted in gaining rough dimensions for the HET enabling the rapid design and development of this laboratory model. The final design utilises a low carbon steel body, a Boron-Nitride discharge channel, three internal solenoid type electromagnets and a 3D laser sintered metal printed anode.

Table 2

A table comparing the tested propellants, where percentages relative to xenon are also shown. It is also important to note that the ionisation energy level shown for nitrogen is for N_2 , in the plasma it is expected that several states of diatomic and atomic nitrogen would be present [16,54].

	Xe	Kr	Ar	Ne	N_2
Mass, amu	131.3	83.8	39.9	20.2	28.0
1st IE, eV	12.1	14	15.8	21.6	15.58 ^a
2nd IE, eV	21.0	24.4	27.6	41.0	*
NA, ppm	0.087	1.14	9340	18.21	780840
Mass, % _{Xe}	–	63.8	30.4	15.4	21.3
1st IE, % _{Xe}	–	115.7	130.6	178.5	128.8 ^a
2nd IE, % _{Xe}	–	116.2	131.4	195.2	*

^aThis value is for $N_2 \rightarrow N_2^+ + e$; not for $N_2 \rightarrow N+N^+ + e$. This has been seen to be the most common ionised state from neutral diatomic nitrogen [55].

3. Effects of propellant selection

Xenon is an excellent propellant for space propulsion, with its high storage density, chemically inert nature, high atomic mass, low ionisation energy (IE), and large ionisation cross sectional area. In Table 2 each tested propellant is shown compared to xenon. The primary drawback of xenon is its low natural abundance (NA), being an order of magnitude less than the next least abundant propellant proposed, krypton.

3.1. Ionisation

The ionisation mechanics of Hall effect thrusters largely influences the plasma properties. As result, several ionisation criteria and relations should be observed for efficient operation. Propellant selection has a large impact on the ionisation dynamics, where the cross-sectional area of ionisation, ionisation energies, and atomic mass, all affect the rate of ionisation for a given operational condition.

The rate of ionisation within a Hall thruster, v_i , can be expressed as,

$$v_i = n_n \langle \sigma_i v_e \rangle \quad (13)$$

where σ_i is the cross-sectional area of ionisation, and v_e is the electron velocity. It is worth noting that $\langle \sigma_i v_e \rangle$ denotes the average accounting for the probability distribution function of the electron velocity and is commonly referred to as the reaction rate; this will be explained in greater detail in Section 3.2.1. The neutral number density of the propellant is a function of propellant atomic mass and velocity, channel size, and mass flow rate and can be calculated by rearranging Eq. (4) such that,

$$n_n = \frac{\dot{m}_n}{A_c m_n u_n} \quad (14)$$

In Section 2.1 the neutral number density was set at the targeted critical value, however here a range of mass flow rates are being investigated such that this value is determined from the mass flow rate, channel geometry, neutral velocity, and propellant. Moreover, the neutral gas velocity that is determined from the neutral temperature will have an impact on how mass flow relates to the neutral number density, adding further importance to the assumed neutral temperature as previously discussed in Section 2.1 [15,45,46].

3.1.1. Cross sectional area of ionisation

The cross-sectional area of electron impact ionisation strongly relates to the performance of the thruster. This is due to the connection of cross-sectional area to the mean free path of ionisation for a given propellant, with sufficient ionisation often described to be met through the Melikov-Morozov criterion. This criterion stipulates that the mean free path of ionisation must be significantly smaller than the ionisation region of the plasma, ensuring that the neutral particles have a high

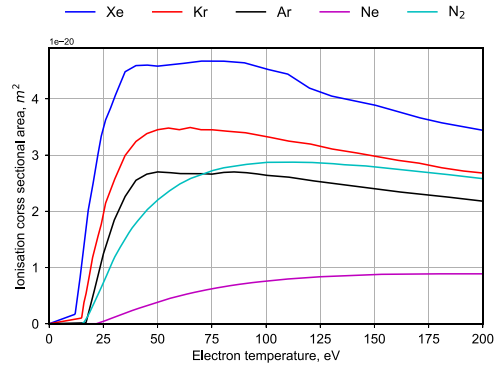


Fig. 5. Cross-sectional area of ionisation for the propellants tested against bulk plasma temperature in electron volts. Cross-sectional area values used are from; Xenon and krypton [57], argon [58], and neon and diatomic nitrogen [59].

probability of an ionising collision before they travel the length of the channel and enter the acceleration region [5,15,39]. This can be described as,

$$\lambda_i \ll L \quad (15)$$

where λ_i is the mean free path of ionisation. The mean free path can be described as the ratio of the neutral propellant's velocity and the rate of ionising collisions such that [5],

$$\lambda_i = \frac{u_n}{n_e \langle \sigma_i v_e \rangle} \ll L \quad (16)$$

where $\langle \sigma_i v_e \rangle$ is the reaction rate and n_e is the electron number density. The electron number density has been found experimentally to be approximately 10% of the neutral number density such; $n_e = 0.1 \times n_n$ [15]. In some applications the mean free path is calculated with neutral number density has been used rather than electron number density. However, for the case of slow-moving particles, neutrals, that are impinged by a volume of high-density fast-moving particles, confined electrons, then Eq. (16) as shown should be used [5].

It should be noted though that this is an oversimplification of the ionisation dynamics of a Hall thruster, as the ionisation region of the plasma does not occur throughout the entire length of the channel but rather in a distinct region of the plasma near the channel exit [14]. In practice there exists a region near the channel exit, where the magnetic field peaks, in which the vast majority of ionisation occurs. Nevertheless, the size of the ionisation region of the plasma is hard to predict with any level of accuracy; with some having suggested that experimental results have shown the size of this region is approximately the channel width, h [14]. This implies that $h \ll \lambda_i$ should also be a strongly controlled parameter in HET design and that there exists a proportionality between ionisation efficiency and channel width of a thruster. However, within HETs the ratio of channel length to width, L/h , generally ranges between 1–2, with $L/h \approx 1.7$ for both the SPT-100 and the Alta 5 kW HET, and $L/h \approx 1.0$ in the MaSMi-60 [4,39,56]. This suggests that the Melikov-Morozov criterion, regardless of use with channel length or channel width, will be mostly unchanged.

The cross-sectional area of ionisation is important for theoretical ionisation estimates, with it illustrated for the considered propellants in Fig. 5. Here it can be seen that xenon has the largest area of ionisation, of the considered propellants, followed by krypton. It can also be seen that both argon and diatomic nitrogen share similar areas and that neon has almost an order of magnitude lower area than xenon. This suggests that argon and nitrogen will ionise at a similar rate, and that neon may be difficult to ionise.

It is also beneficial to note that diatomic nitrogen has been shown to more readily ionise to $N_2 \rightarrow N_2^+ + e$ than $N_2 \rightarrow N^+ + e+N$ [55,60]. This is due to N_2^+ having $> 4x$ larger cross-sectional area of ionisation than that of both N^+ and N_2^{++} combined [60]. Moreover, N_2 has a

large dissociation energy of 9.8 eV meaning the threshold of electron energies that could cause dissociation is only slightly lower than that of ionisation [54]. Compare this to iodine, a promising alternative propellant to xenon that is also diatomic prior to ionisation, which has a dissociation energy of only 1.54 eV. As a result, within an iodine fuelled Hall effect thruster plasma discharge it is expected that the exhausted propellant will be fully dissociated and as a result should be treated as a mono-atomic propellant [61]. This differs for a nitrogen fuelled Hall thruster plasma where the exhausted ions should be treated as diatomic.

3.2. Mass

Xenon has a strong legacy as the standard propellant for electric propulsion due to several factors. The propellant selection effects several key aspects of the operation of HETs and the plasma properties, with the main impact of propellant selection being the ionisation dynamics of the neutral atoms. Furthermore, thrust, and specific impulse output of the thruster, is strongly tied to the atomic mass of each propellant, such that for a constant discharge voltage;

$$T = \frac{d(m_n v_e)}{dt} = \dot{m}_n v_e = \underbrace{\frac{\dot{m}_n I_d}{q}}_{v_e} \sqrt{\frac{2qU_d}{m_n}} \quad (17)$$

$$= I_d \sqrt{\frac{2m_n U_d}{q}} \propto \sqrt{m_n}$$

and for specific impulse,

$$I_{sp} = \frac{T}{g_0 \dot{m}_n} = \frac{I_d \sqrt{\frac{2m_n U_d}{q}}}{g_0 m_n I_d \frac{1}{q}} = \frac{1}{g_0} \sqrt{\frac{2qU_d}{m_n}} \propto \frac{1}{\sqrt{m_n}} \quad (18)$$

where v_e is the ion exit velocity, q is the ion charge and I_d is the discharge current. This shows that the thrust and specific impulse are proportional and inversely proportional respectively to the square root of atomic mass of the propellant used, for a constant discharge voltage.

Xenon's large atomic mass is also beneficial for efficiency for a given constant specific impulse [46]. If the efficiency of the thruster, η , can be described by the kinetic energy of the exhaust and the total potential loss factor Φ_L such as,

$$\eta = \frac{\frac{1}{2} m_i c^2}{\frac{1}{2} m_i c^2 + e\Phi_L} = \frac{c^2}{c^2 + \frac{2e\Phi_L}{m_i}} \quad (19)$$

where Φ_L is assumed constant here for a given specific impulse, however in practice this value is likely voltage and propellant dependent. From this it can be seen that as the atomic mass of the propellant is increased, the impact of the loss factor is minimised for a constant specific impulse, maximising η [46]. Moreover, the large atomic mass of xenon prevents the trajectory of the ions being affected by the magnetic field present. Significantly lighter propellants would suffer acceleration losses from non-axial velocity incurred from the ion paths being curved by the magnetisation of the ions.

In Table 2, the atomic mass of suggested alternative propellants is shown. Eq. (17) and (18), suggest that for the same power if a low atomic mass propellant like neon is used instead of xenon, an extremely high specific impulse could be achieved for the same discharge voltage. However, this increase in specific impulse is often offset by a decrease in thruster efficiency through a lower mass utilisation efficiency.

To define mass utilisation efficiency a definition for ionisation efficiency, α , is required. This is defined as the ratio of ion current in the plume to the "neutral" current, the theoretical maximum amount of singularly charged ions that can be produced through perfect total ionisation;

$$\alpha = \frac{I_b}{I_{\dot{m}_n}} = \frac{\bar{q}\dot{m}_i}{e\dot{m}_n} \quad (20)$$

where I_b is the beam current, $I_{\dot{m}_n}$ is the injected "neutral" current, and \bar{q} is the average charge of the exhaust.

As a result, the mass utilisation efficiency is given as the ratio of ion mass to neutral mass injected,

$$\eta_m = \frac{\dot{m}_i}{\dot{m}_n} = \frac{I_b}{e} \frac{m_n}{\dot{m}_n} = \alpha \frac{\bar{q}}{e} \frac{m_n n_n}{\dot{m}_n} \quad (21)$$

where \dot{m}_i is the ion mass flow rate, I_b is the beam current, \bar{q} is the average ion charge, n_n is defined in Eq. (14), and α is the ionisation efficiency. For a constant neutral number density anode mass flow rate decreases proportionally with propellant mass, such that the dominating factor of this equation is the ionisation efficiency, which decreases for harder to ionise propellants. Given that less massive propellants are generally harder to ionise it is expected that mass utilisation will decrease. Some exemptions to this logic are iodine, zinc, and magnesium as each have a lower ionisation energy than xenon whilst being less massive [27,36,62]. However, the impact of ionisation energy is not directly described and might not strongly impact the overall efficiency of Hall thrusters.

As well as ionisation considerations, the atomic mass of the selected propellant has a significant impact on the neutral gas dynamics within a Hall effect thruster. As previously discussed in Section 2.1, it is assumed that the neutral particles travel with a thermal velocity resulting from the anode temperature. As can be seen in Eq. (2), this velocity has an inverse square root proportionality to the mass of the selected propellant. For example, for the same assumed anode temperature the ratio of xenon's and krypton's neutral velocity is $u_{n_{Xe}}/u_{n_{Kr}} \approx 0.8$. This will inevitably have a significant impact upon the mean free path of the propellant as can be seen in Eq. (16). For a less massive propellant the neutral atoms will transit through the ionisation region of the thruster in a shorter time period, further reducing the ionisation rate for the same thruster geometry.

The effect on the mean free path by altering anode voltage and the assumed neutral temperatures can be seen in Fig. 6, with argon, krypton, and xenon shown. It is clear that the assumed anode temperature and by extension the neutral temperature has a significant effect upon the calculated mean free path.

The relationship between neutral temperature and mean free path will have an increased sensitivity for propellants that are lighter or operating at a lower voltage. Lower atomic mass propellants also have a greater sensitivity to changes in voltage due as this will decrease the bulk electron temperature and in-turn cause a greater reduction to ionisation cross-sectional area, as can be seen in Fig. 6. In addition, the effect of anode voltage and propellant selection can also be seen here. Given this strong relationship, it would seem reasonable to assume that the propellant mass should be more integrated into the scaling relationships, while also suggesting the assumption of the anode temperature is overly simplistic.

3.2.1. Reaction rate coefficients

To calculate the reaction rate, $\langle \sigma_i v_e \rangle$, the resultant product of probabilistic velocity of the electrons at the bulk plasma electron temperature, and the cross-sectional area of inelastic interaction for neutrals in the plasma need to be considered. This can be approximately estimated by an integration of the Maxwellian-Boltzmann distribution of the microscopic electron velocity of thermal origin, defined as w , which can be used to arrive at a reaction rate coefficient [63]. The 3-dimensional velocity, w , described independent of the directional velocity is,

$$g(w, T_e) = \sqrt{\frac{2}{\pi}} \left(\frac{m_e}{K_B T_e} \right)^{3/2} w^2 \exp \left[-\frac{m_e w^2}{2 K_B T_e} \right] \quad (22)$$

where $g(w, T_e)$ is the Maxwellian-Boltzmann electron velocity distribution function, and m_e is the electron rest mass. This integral can be expressed as a function of bulk electron temperature [45,63],

$$\langle \sigma_i v_e \rangle(T_e) = \int_0^c w \sigma_i(T_e) g(w, T_e) dw \quad (23)$$

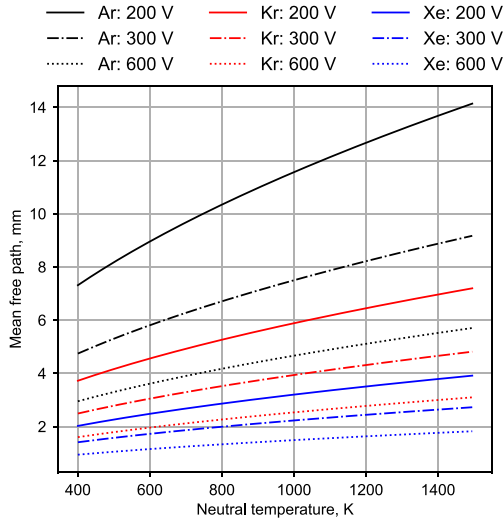


Fig. 6. A plot showing the variation of the mean free path for xenon, krypton, and argon at three anode voltages, 200 V, 300 V, and 600 V for a range of assumed neutral temperatures. This calculation was undertaken with the assumption of optimal neutral number density of $n_{n,c} \approx 1.2 \times 10^{19}$ as previously discussed in Section 2.1.

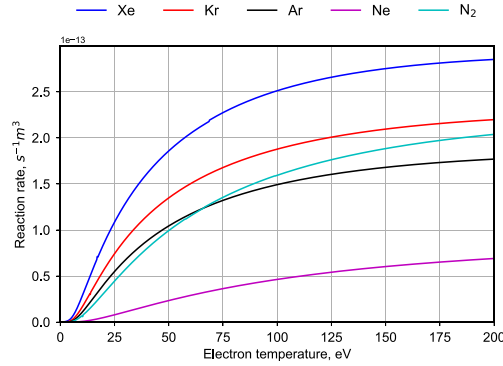


Fig. 7. Computed reaction rate coefficients, for each propellant tested, against bulk plasma temperature in electron volts.

Table 3

A comparison between the reaction rate coefficient and the cross-sectional area for each tested propellant at the expected plasma temperature for a 300 V discharge voltage [15].

	Xe	Kr	Ar	Ne	N ₂
$\sigma_i, 10^{-20} \text{ m}^2$	4.01	2.55	1.84	0.12	1.17
$\langle \sigma_i v_e \rangle, 10^{-14} \text{ m}^3 \text{s}^{-1}$	13.6	8.85	6.33	0.96	5.16
$\sigma_i, \%_{Xe}$	–	63.6	45.9	2.9	29.2
$\langle \sigma_i v_e \rangle, \%_{Xe}$	–	65.0	46.5	7.1	37.9

where c is the speed of light and taken as the upper bound for electron velocity. Eq. (23) was solved numerically, the results of this calculation for elements under consideration can be seen in Fig. 7.

For all tested propellants a peak reaction rate per electron temperature is present; these peaks are: Xe: 25.3 eV, Kr: 28.9 eV, Ar: 31.6 eV, Ne: 68.5 eV and N₂: 42.8 eV. This highlights the point of diminishing returns for increased plasma electron temperature for ionisation is reached earlier for xenon. Although, the variation between peak reaction rates is relatively small in magnitude with krypton, argon and nitrogen being relatively similar values of reaction rate per electron volt. This highlights that the most efficient extraction of reaction rate occurs at plasma temperatures that would be present within 200–400 V discharges.

Table 3 illustrates calculated cross-sectional areas and reaction rates for a thruster operating at an assumed discharge voltage of 300 V, corresponding approximately to an electron temperature of 36 eV [15].

As can be seen in Table 3 and Figs. 5 & 7, xenon clearly has the largest cross-sectional area and reaction rate. This is followed by krypton, then argon and nitrogen that has relatively similar magnitudes and distribution, and neon that has significantly lower values than all other considered propellants.

Due to the similar mass and ionisation energy, see Table 2, and similar reaction rate coefficient curves, it can be suggested that diatomic nitrogen will operate comparably to argon for similar mass flow rates.

3.3. Theoretical performance

To better illustrate the effect of propellant selection on performance, the theoretical state-space for the propellant's ionisation efficiency can be constructed for a common thruster geometry. For this comparison the HEKT-100's geometry was used to allow for deeper understanding of the ionisation limits in the thruster operation orientated metrics of anode voltage and anode mass flow rate.

The ionisation efficiency as described in Eq. (20) can also be described as an exponential function in the form,

$$\frac{\dot{n}_i}{\dot{n}_n} = \alpha = 1 - \exp\left[-\frac{L}{\lambda_i}\right] \quad (24)$$

This function describes the ratio of the neutral anode flux that is ionised given a transit through a specific plasma thickness, assumed here as the channel length L , for a constant mean free path, λ_i [41]. This evaluation however only considers singularly charged ions, such that $\bar{q} = e$. This equation can be used in channel length scaling by setting $\alpha = 0.8$ and then calculating the mean free path via Eq. (16), a channel length can then be selected to satisfy Eq. (24) [15]. Alternatively, α can also be used to investigate and compare different propellant's operating envelope for that same geometry.

Note that Eq. (24) uses the entire channel length, L , whereas previously discussed in Section 3.1.1, this is stated as a poor assumption of the length that ionisation occurs over and rather an ionisation layer thickness should be computed. However, due to the complexity and uncertainty in calculating this shorter ionisation length value, here the entire channel length is used.

The ionisation efficiency can also be used in an estimate for the anode power of the thruster. The Anode power of a Hall thruster can be described with;

$$P = U_d I_d \quad (25)$$

where I_d is the discharge current. Discharge current can be expressed in terms of the ion flux of the thruster such that,

$$I_d = \frac{\dot{m}_i \bar{q}}{m_i} = \frac{\alpha \dot{m}_n e}{m_n} \quad (26)$$

where, \dot{m}_i is the ion flux that result from ionisation of the neutral "current" \dot{m}_n such that $\dot{m}_i = \alpha \dot{m}_n$. Moreover, only singular charged ions are considered such that $\bar{q} = e$ is true. Using Eqs. (25) and (26) the power for a Hall thruster can be described as,

$$P = U_d I_d = \alpha U_d \frac{\dot{m}_n e}{m_n} \quad (27)$$

From this the target power of the thruster can be displayed alongside the ionisation efficiency values.

Fig. 8, shows a state space of the HEKT-100 Hall effect thruster in terms of the ionisation efficiency as flow rate and anode voltage are varied. This state space has been constructed for each of the five propellants being considered. This, while a very idealised model, does give insight into the ionisation and limitations imposed for various propellants. It is suggested that any region where $\alpha < 0.8$ would not satisfy the Melikov-Morozov criterion and result in poor ionisation, and therefore in unsustainable plasma characteristics. Although, given the many ideal assumptions included within this analysis the criterion of $\alpha \geq 0.8$ is too optimistic and any value of $\alpha \leq 0.99$ is suggested to be likely inoperable or an unstable state.

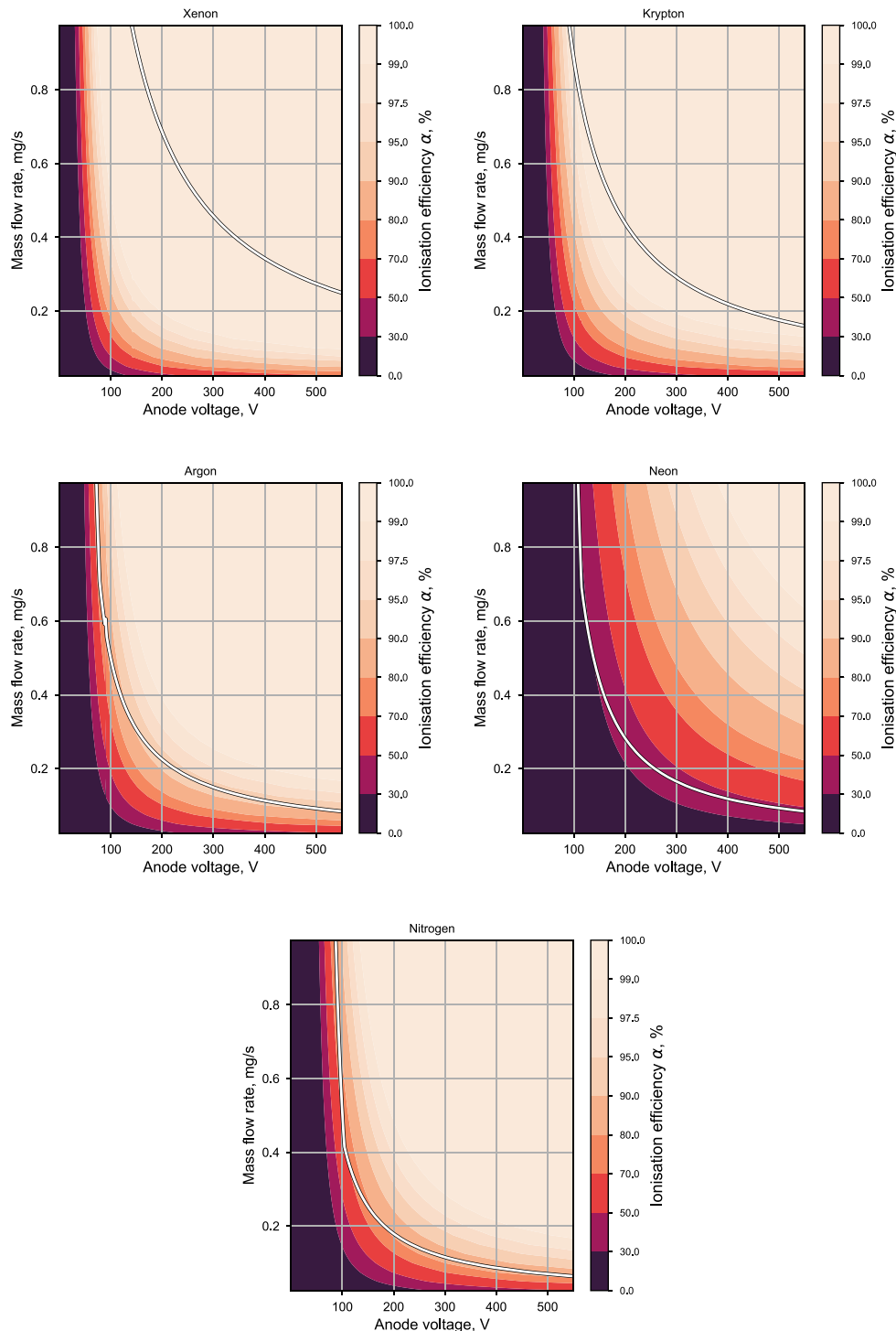


Fig. 8. Contour plots for the HEKT-100 of propellant efficiency, α , against anode mass flow rate and voltage. The white line indicates where a 100 W anode power discharge would be expected, calculated using Eq. (27).

As can be seen, xenon is clearly readily ionisable, with the vast majority of the state space satisfying $\alpha > 0.8$. This is expected as the HEKT-100 was designed for operation with krypton, although xenon would naturally be readily ionised in a krypton optimised environment. Furthermore, the large atomic mass of xenon results in longer transit times, and the large reaction rate resulting in short mean free paths.

Krypton, argon, and nitrogen all exhibit similar distributions and magnitudes of ionisation efficiency, suggesting that each one will operate in similar envelopes. Although a larger variation should be expected

in practice as this model omits several aspects of Hall thruster operation that would impact ionisation efficiency characteristics. One example being, electron impact ionisation energies, an energy loss mechanism that would depend on the ion number density, which is greatly increased for lower atomic mass propellants for equal mass flux. Moreover, as can be seen in Table 2, lighter propellants require greater energies for ionisation due to the electron shells in lighter elements being closer to the nuclei. This would result in greater energy losses from the plasma to the propellant resulting in reduced the plasma temperature—further reducing the ionisation rate.

As the ionisation efficiency is calculated from the mean free path as can be seen in Eq. (16) this data is strongly related to Fig. 7. However here this data is now displayed in a thruster geometry dependent form for specificity the HEKT-100. Following accounting for atomic mass and thruster-specific geometry, it is far easier to observe the shrinking gap in performance between krypton, argon, and diatomic nitrogen. Moreover, it shows how changing the propellant makes operation at low power impossible for lighter propellants within this thruster geometry. For example, neon fails to satisfy $\alpha \approx 0.8$ for the vast majority of the state space. Moreover, for neon it clearly shows that operation at 100 W would likely be impossible within this geometry.

This is a relatively naïve model that neglects several other factors within ionisation and primarily focuses on the mean free path. This can be seen in increasing neutral number densities purely being considered to benefit ionisation, and only considering singly charged ions.

It is worth noting the thruster was designed for a discharge voltage of 300 V at a mass flow rate of 0.354 mg/s of krypton [36]. The range of mass flow rates and voltage seen in Fig. 8 were chosen to mirror the experimentally tested envelope.

The design target discharge power of 100 W is highlighted on each plot in Fig. 8 for the respective propellant. This highlights that for the constant geometry of the HEKT-100 the lighter propellants argon, neon, and nitrogen all have 100 W lines below $\alpha < 0.99$ and in neon's case even below 0.8. This is due to the lighter propellants having greater neutral number densities for the same mass flux and thus increasing the number of ions per unit mass of propellant. This shows that for lower mass propellants operating within the same geometry higher discharge powers are required for stable operation, and that if low powers are to be targeted with alternative propellants, alterations to the thruster design must be made.

3.4. Channel length scaling

The channel length for this thruster was chosen to be 32.4 mm, as discussed in 2.1. This length was chosen such that the geometry would satisfy the Melikov-Morozov criterion as described in Eq. (15). This criterion states that the mean free path of the neutral propellant must be significantly shorter than the ionisation region, assumed to be equitable to channel length for scaling purposes. However as discussed in Section 3.1.1 there are significant limitations to this assumption. Channel lengths for extensively tested xenon Hall thrusters are typically within the range of 5–20 mm, however some thrusters have larger channel lengths [4,29,39,47,64–67]. These thrusters are thought to be following this convention, and as such this criterion is the primary way with which channel length sizes are evaluated.

The Melikov-Morozov criterion when considering alternative propellants creates additional complexities, such that, as the neutral mass of the propellant decreases there is also an expected decrease in the cross-sectional area of ionisation, as seen in Fig. 5. The mean free path will increase significantly for less massive propellants due to reduced ionisation and reduced transit times for the neutral propellant within the plasma, as shown in Fig. 6; suggesting a longer channel will result in improved ionisation. However, as shown by E. Azevedo, a parametric study was undertaken for a Water (vaporised H₂O) fuelled Hall thruster with a range of channel lengths. In this study it was found that a longer channel did not improve thruster performance, going against the conventional logic as proposed by the Melikov-Morozov criterion [68]. Whilst this study is small in scope, testing only one thruster and two channel lengths, this result seems to completely go against the convention of sizing channel length via the Melikov-Morozov criterion. The increased channel length may assist in ionisation, however there might also be larger implications to performance when large channel lengths are used, specifically when alternative propellants are being considered. Channel length would affect the heating and propagation of neutrals through the thruster which will influence thruster operation. It is known that the ionisation region does not span the entire channel

length, as previously discussed, such that increasing this channel length beyond a point would not increase ionisation [14]. As previously discussed in Section 3.1.1, It is possible that preserving a close to unity L/h ratio is more practical application for channel length scaling than satisfying the Melikov-Morozov criterion with channel lengths that exceed channel width significantly.

The design of the HEKT-100 aimed to satisfy the Melikov-Morozov criterion with a long channel length that results in a L/h ratio of 6.5, as can be seen in Table 1. This long channel length may have negatively impacted the performance of this thruster and such that future scaling of Hall thrusters should develop a more comprehensive method for scaling channel lengths than the Melikov-Morozov criterion, which while an important criterion, is likely overly simplistic. Moreover, once alternative propellants are being considered the suggested length scales of the thruster geometry become excessive and no longer represents the ionisation region effectively; as a result, an alternative method will be needed to effectively capture an efficient design methodology.

4. Experimental method

4.1. Vacuum chamber

The testing was carried out in the large vacuum chamber facilities at the University of Southampton. The 2.0 m diameter 4.5 m long chamber is equipped with one Oerlikon Leybold LV140C roughing pump, two Coolpower 140T cryo compressors and two Coolpack 6000H 20K cold heads, and two MAG W 2200 iP magnetically levitated turbopumps. With an ultimate achievable vacuum of $< 9 \times 10^{-8}$ mbar and an operational pressure of $< 5.0 \times 10^{-5}$ mbar with 28 sccm of xenon injected.

4.2. Cathode

The cathode used for the entirety of the testing was a “Model 5000 Hollow cathode electron source” from IonTech, a cathode capable of providing 0–20 amps. The cathode uses a tungsten filament for electron emission and can be seen mounted in Fig. 4 and Fig. 9 on the bottom side of the image, it can be seen more clearly in the neon discharge.

This is not a space grade cathode and requires non-negligible mass flow rate of propellant to operate, the nominal operation with this cathode being conducted with 0.49 mg/s of krypton. This suggests that at low anode flow rates significant ingestion of neutrals and ions from the cathode plume could be occurring, artificially increasing the performance of the thruster. Moreover, some xenon tests, and all nitrogen and neon tests, were conducted with 0.29 mg/s of xenon to the cathode. There was no effect on thruster performance observed between krypton and xenon fed cathode for the xenon and krypton thruster testing. However, an investigation into the cathode flow rate effects on thruster performance was undertaken and are described in Section 6.

4.3. Thrust stand

The thrust stand used is a pendulum type thrust stand with no passive or active dampening, utilising a laser triangulation displacement sensor [36].

The thrust stand was modified and re-calibrated several times during the testing campaign. The calibration coefficient for each run underwent statistical error analysis as outlined by J. Polk et al. [69] where the calibration error for the thrust stand ranged between 1.3–6.1% and with a resolution of thrust measurement error between 0.22–2.0 mN. Moreover, the thrust balance showed good repeatability with data points being taken at similar power and mass flow rates showing close agreement even between calibration cycles.

5. Experimental results & discussion

For the purpose of evaluation, the thrust, specific impulse, and anode efficiency are compared. The specific impulse is calculated from

thrust stand measurements using;

$$I_{sp} = v_{ex} \frac{1}{g_0} = \frac{T}{\dot{m}_a g_0} = \frac{T}{\dot{m}_a g_0} \quad (28)$$

The anode efficiency is calculated using;

$$\eta_a = \frac{P_{jet}}{P_{anode}} = \frac{\frac{1}{2} \dot{m}_a v_{ex}^2}{P_{anode}} = \frac{T^2}{2\dot{m}_a P_{anode}} \quad (29)$$

where P_{jet} and P_{anode} are the jet (or plume) kinetic power and the anode power respectively. Eq. (28) and (29) are both used to compute I_{sp} and anode efficiency directly from thrust for the following data.

Thrust measurements were taken via the measurement of pendulum displacement whilst active and whilst powered down. This displacement is then computed into thrust directly via a calibration coefficient.

Testing was performed on several separate occasions where the thruster has been disassembled and non-active for several months at a time. Chronologically krypton was tested first, followed by xenon and argon. Then, after several months, additional xenon testing followed by neon and finally nitrogen. For all tests the same magnetic configuration was maintained with 2.42 A of current being provided to the main coil. The current to the magnetic circuit only being altered to enable operation at very low powers.

5.1. Observations

Thruster operation was imaged for all propellants tested, a side by side of each tested propellant can be seen in Fig. 9. This allows for a somewhat anecdotal comparison on the visual operation. There was not an overlap in powers and mass flow rates for each propellant shown in Fig. 9; such a direct comparison cannot be drawn.

For neon and nitrogen discharges shown in Fig. 9, the operation was conducted with higher mass flow rates to ensure ignition; as a result, a comparatively large plume is seen. The krypton discharge demonstrates the smallest plume, due to the lower power levels used. As the thruster was designed specifically for an ≈ 100 W discharge with krypton here the image shows that level.

One of the many effects of altering the propellant in the operation of a Hall effect thruster is the differing relationship between mass flow rate and neutral number density of the propellant, as a less massive propellant will have a high number density for the same total mass flux. This relationship can be seen in Fig. 10, where the tested range of mass flow rates for each propellant is denoted by the solid line. It is important to note that the maximum mass flow rate of the argon testing was experimentally limited due to the propellant delivery system being limited volumetrically and not necessarily an operational limitation of the design. For neon and nitrogen testing a higher flow capable mass flow controller was used for the propellant delivery system.

For the majority of the testing the anode power did not exceed 400 W with very brief testing at powers above this value. Below anode powers 300 W no thermal issues were apparent, however above this value resistance increase in the electromagnetic coils was observed such that these power levels were not maintained for long durations.

5.1.1. Xenon

Xenon was the most prolifically tested propellant due to the ease of use as well as a method of evaluating the thruster's performance. As there was a period of disuse of the thruster, a second xenon test sweep was undertaken to confirm similar operation and performance. The testing with neon and nitrogen could be undertaken knowing that any measured differences were exclusively due to the change in propellant.

Unsurprisingly, xenon performed well as a propellant in this thruster, achieving the highest thrust, anode efficiency and specific impulse of the propellants tested which has been seen before in literature [21,39]. Furthermore, as it can be seen in Fig. 15, there is no plateau in the performance as voltage or power increases, suggesting that the optimal performance for each flow rate tested could be at higher powers than tested.



Fig. 9. Side by side comparison of the thruster operating on each propellant tested. Bottom to top: Xenon, krypton, argon, neon[‡], and nitrogen.

‡: There is an unknown non-negligible amount of xenon also present in the neon discharge.

5.1.2. Krypton

Krypton was the first propellant tested, as discussed in previous work [36]. General performance was good with plateauing of the thrust for a given flow rate. This suggests that the maximum potential performance for that given flow rate was achieved.

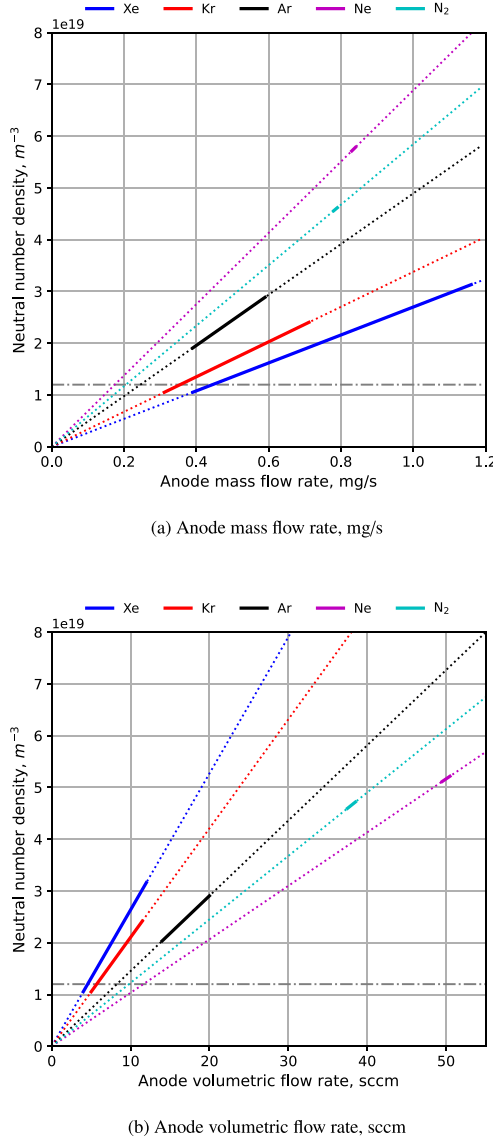


Fig. 10. Relationship between the anode mass and volumetric flow rate and the neutral number density for the HEKT-100, created with Eq. (14) and at an assumed neutral gas temperature of 800 K. The dash-dot line represents the relationship over the minimum and maximum tested flow rate, whilst the solid line represents the actual tested anode mass flow rates. The horizontal black dashed line represents the critical neutral number density as proposed by Dannenmayer et al. [15,40].

As the plateauing was observed with krypton and not xenon, this suggests that the thruster designed for krypton was indeed optimised for extracting krypton's potential at the designed power. Moreover, from literature it is expected that krypton anode efficiencies will be approximately 5%–15% lower than that of xenon for the same thruster geometry [21]. Here the difference at the designed operational power of 100 W between xenon and krypton discharges is $\approx 6.3\%$, at a discharge voltage of approximately 250 V. This small change suggests further that the thruster was successfully designed for krypton at that power. This smaller disparity could also be a result of the design favouring krypton operation and as a result xenon is significantly under-performing in this thruster, reducing this disparity in performance that is normally seen in xenon optimised thrusters operating on krypton [21].

5.1.3. Argon

Argon was tested successfully with a more limited operational envelope. This was due to the higher volumetric flow rate required for



Fig. 11. Thruster operating on neon within the large vacuum chamber facilities at The University of Southampton.

operation. Due to the constant channel width, at the higher flow rates, the neutral number densities that are present are much greater than for equivalent anode mass fluxes with xenon or krypton. The effect of varying the mass flow rate and the resulting neutral number densities for this thruster can be seen in Fig. 10.

It is suggested that as the neutral number density goes above this “critical” value, found empirically, the increased frequency of electron-atom collisions result in increased electron diffusion along the magnetic field which in turn results in weakened magnetic confinement of the electrons. This process would allow more electrons to back stream through the channel reducing efficiency [15,40]. The lighter atomic mass of argon would also contribute to the lower performance measured. If the ionisation region is assumed to remain constant between propellants the lighter argon would have a shorter transit time and thus a reduced ionisation efficiency. Moreover, argon will be more sensitive to neutral gas temperature due again to the reduced mass when compared to xenon or krypton.

Generally, argon showed slightly reduced thrust and specific impulse than that of krypton. This minor loss could be due to the higher ionisation energy of argon and reduced efficiency due to the high number densities present increasing anode current draw [40]. Moreover, the shorter resistance time of the argon would negatively impact the ionisation efficiency.

5.1.4. Neon

Neon was ignited successfully several times during this testing. This was achieved by first filling the propellant lines with xenon, then opening the neon propellant feedline. This would allow for the thruster to ignite under pure xenon and transition into neon operation as the remaining xenon was consumed. This transition was visible in the substantial colour change and drop in the extracted current as the harder to ionise neon became the dominate propellant present.

This method of ignition would cause the thruster to draw anode powers much greater than what were considered in the design, specifically in terms of the thermal load, during the majority xenon phase of the propellant transition. Under this transient operation the peak power draw at ≈ 850 W at approximately 650 V. The thruster was not operable under pure neon operation, as shortly after the dominate plasma colour became an intense neon-red hue, the anode current draw would rapidly drop, over the span of several seconds. The plasma would ignite and eventually extinguish when the xenon was exhausted, or the concentration became too low to continue assisting in ionisation.

The initial ignition to a xenon blue “glow discharge” plasma occurred under a low voltage current limited state. As more neon entered the anode and was ionised the voltage would quickly climb to the limited 650 V, this was also accompanied by the mode transformation



Fig. 12. Thruster operating on nitrogen within the large vacuum chamber facilities at The University of Southampton.

into an “accelerating plasma” discharge, as seen in Fig. 11, where significant increase to thrust and change in plume shape was observed. From here the current would begin to drop but the plasma extinguished quickly once below 1 A of anode current draw.

Several data points were taken under unstable transient operation, although these data points will likely not accurately represent the thruster’s steady state performance. Moreover, there was no method of determining the xenon percentage at the time of thrust measurements. As a result, the thrust measurements obtained whilst under neon operation are omitted. The thrust levels acquired were also consistent for a xenon discharge at those powers; further suggesting that the dominate contributor to the thrust was the xenon.

Without a steady operational mode achieved at the highest powers tested and, being unwilling to increase the discharge voltage further, neon testing was concluded.

5.1.5. Nitrogen

Nitrogen, as suggested in Section 3, was similar in operation to argon. Initially ignited similarly to neon with a large mass flow used, once it was established the thruster could self-ignite under pure nitrogen conditions, the addition of xenon for ignition was stopped. Due to the large flows used during operation the plume size of the thruster is of a similar size as during the neon testing, which can be seen in Fig. 12.

Unfortunately, the thruster only operated for a few hours under nitrogen operation, due to the failure of the main outer electromagnetic coil. It is believed that the majority of the damage was incurred from the large thermal load during the neon testing.

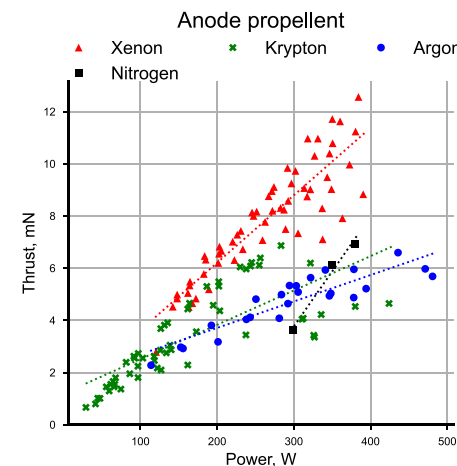
Due to the premature ending of nitrogen testing, only three data points were collected. Each point was taken under steady operation with pure diatomic nitrogen, with xenon fuelling the cathode. It should be noted though that the thruster failed before testing at lower powers making a direct comparison between nitrogen and the other propellants difficult.

With an electromagnet failing during nitrogen testing, there is little confidence in the magnetic field intensity for these tests. As the magnetic field degraded the electron confinement was reduced, and performance decreased.

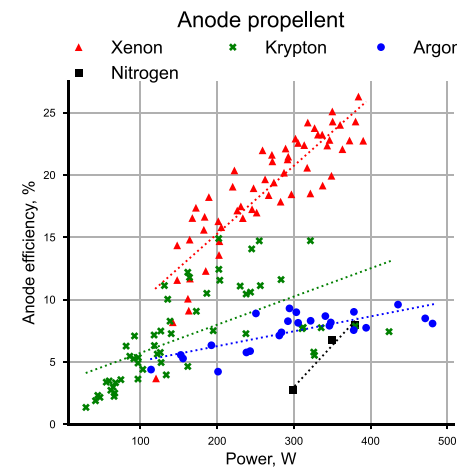
5.2. Grouped comparison

Comparing the performance of each propellant directly in Fig. 13 (across different flow rates and magnetic field configurations), it can be seen clearly that xenon performed the best, with surprisingly little difference between the other tested propellants. For example, the nitrogen performance values are similar to that achieved with argon.

This is backed up by the similar performance from the xenon-doped neon and the pure xenon operation if extrapolated to the same power



(a) Thrust of each propellant successfully tested against anode power.



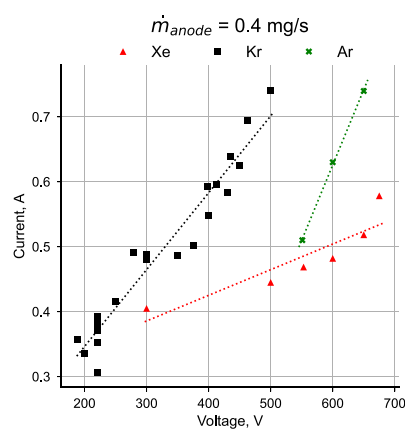
(b) Anode efficiency of each propellant successfully tested against anode power.

Fig. 13. Thrust measured for all propellants successfully tested, all mass flows and voltages tested are shown for each propellant. It is worth noting that the magnetic configuration for the nitrogen data is unlike that of all other data shown here as these tests were conducted as the large electromagnet was failing reducing electron confinement. As a result, direct comparison is not recommended for the nitrogen data.

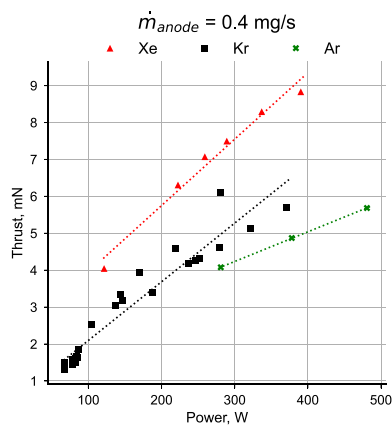
level. However, a direct comparison cannot be made as the xenon testing did not extend to the same anode powers that the neon data was measured at.

As can be seen in Fig. 14(c), the specific impulse for argon is lower than that of both xenon and krypton. As argon has a lower mass, this goes against the implications of Eq. (18). However, as previously discussed, the ionisation rate of argon is expected to be lower than that of both xenon and krypton due to the smaller ionisation cross sectional area and higher ionisation energy. This reduced rate of ionisation is compounded due to the low mass neutral argon atom having a shorter transit time through the thruster geometry. This can be seen with Eq. (2) and visually in Fig. 6 as for all assumed anode temperatures the mean free path for argon is significantly higher than that of both krypton and xenon. This reduced ionisation rate very likely reduced the thruster’s mass utilisation efficiency for argon and as a result the theoretically higher specific impulse is not being achieved.

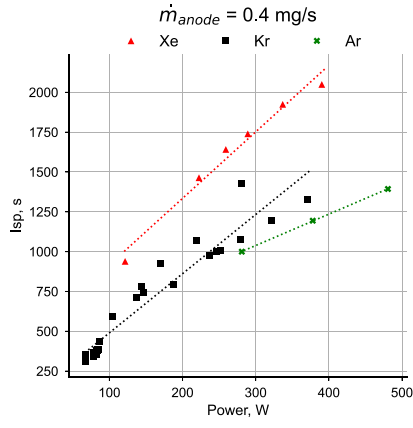
Furthermore, as can be seen in Fig. 10 for the same mass flow of 0.4 mg/s there is significant deviation in the expected neutral number densities present within the channel for each propellant. This can be quantified with Eq. (14) and several assumptions previously discussed



(a) Voltage current behaviour for xenon, krypton and argon all operating at 0.4 mg/s mass flow rate.



(b) Thrust measured for xenon, krypton, and argon against anode power for 0.4 mg/s mass flow rate.



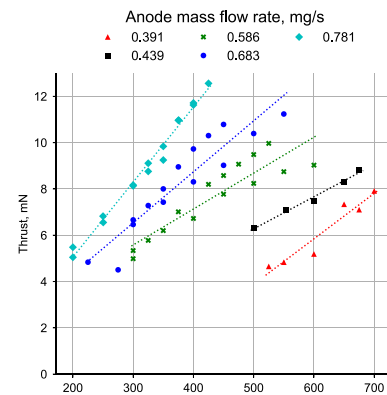
(c) Specific impulse for xenon, krypton, and argon against anode power for 0.4 mg/s mass flow rate.

Fig. 14. The performance of the HEKT-100 on Xeon, krypton, and argon for equal anode mass flow rate of each propellant.

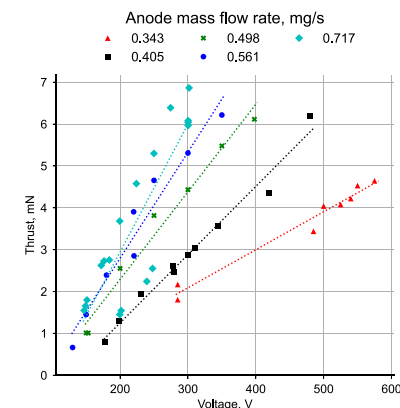
in Section 3, that for the same conditions and 0.4 mg/s the neutral number densities within this thruster are 1.1×10^{19} , 1.4×10^{19} and 2.0×10^{19} for xenon, krypton, and argon respectively. From this it can be seen that argon operation had almost twice the number density for the same mass flux of xenon, which likely impacted performance negatively, as previously discussed in Section 5.1.3. As suggested by [15], at high

neutral number densities magnetic confinement of the electrons can be disrupted due to the high electron–atom collision frequency. This reduction in electron confinement can cause the electric field to expand and reduce in strength, in turn reducing the potential drop accelerating the ions as well as increasing the beam divergence. Both of these factors are likely contributing to the lower than theoretical specific impulse exhibited by argon.

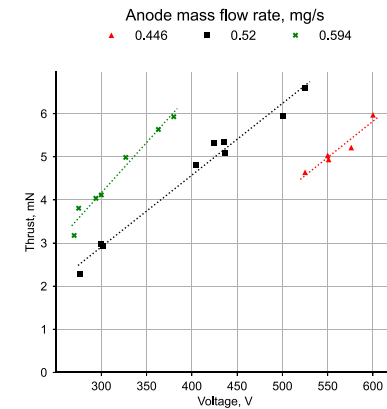
5.3. Thrust measurements



(a) Xenon



(b) Krypton



(c) Argon

Fig. 15. Thrust generated for a given voltage at various flow rates for each propellant successfully tested.

For the purpose of legibility not all collected data is shown.

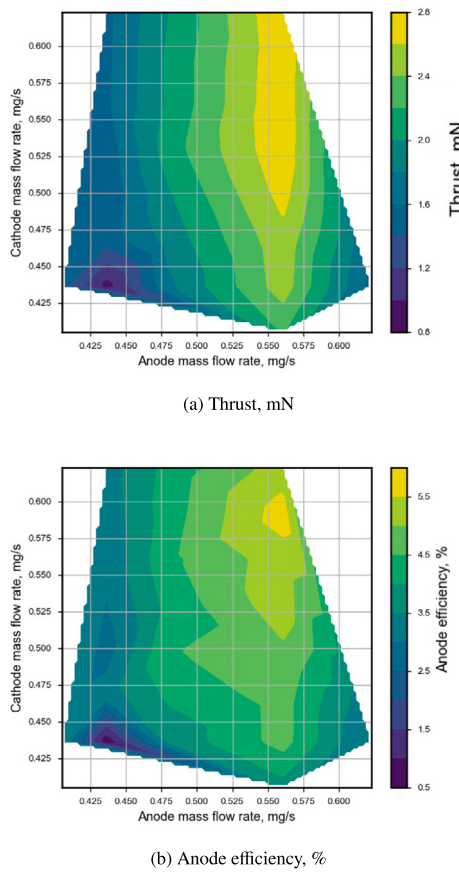


Fig. 16. These plots show the thruster's performance at anode voltage of 220 V as a heat map against both anode and cathode mass flow rates. For this data only krypton was tested for both the anode and cathode.

6. Effect of cathode flow on performance

The cathode used for testing, as previously described in Section 4.2, is the “Model 5000 Hollow cathode”. This cathode requires a significantly higher mass flow than a space grade cathode, which could result in significant ingestion of neutral gas or ions into the HET and alter the performance. As a result, it was important to test the performance effect that the cathode flow rate has on the HET during operation.

Fig. 16 illustrates the performance variation as both the cathode and anode mass flow rates are altered. For all data presented the thruster anode voltage was 220 V and the current was uncontrolled.

The results show that the cathode flow has an impact on the performance of the thruster, although only to a limited degree. As previously mentioned in Section 4.2, for testing where both krypton and xenon were used, the cathode flow rate was limited to 0.49 mg/s and 0.29 mg/s respectively.

7. Conclusion

Work done at the University of Southampton has successfully demonstrated the operation of a low power Hall effect thruster across a wide range of gaseous propellants. The xenon performance recorded is below current commercial thrusters of similar power regimes, suggesting that the performance achieved with all propellants could be improved significantly with further redesigns.

The thruster was operated between 30 W and 810 W with five propellants with mass flow rates ranging 0.31 mg/s to 1.17 mg/s. Peak performance was experienced with xenon propellant with reduced

efficiencies on all other tested propellants. Argon and diatomic nitrogen showing very similar performance as suggested by theoretical evaluation was confirmed experimentally.

Due to the small decrease in performance between krypton and argon, this suggests that a thruster designed and optimised for argon or diatomic nitrogen could outperform krypton for specific impulse with additional cost savings. The main limitation of argon and diatomic nitrogen in this thruster is likely the high neutral number densities negatively impacting the ionisation mechanics [15].

Neon was successfully ignited although due to the low cross-sectional area of ionisation and low reaction rate coefficient, even at high flow rates, steady operation was not achieved. Future work aims to investigate harder to ionise propellants with accurately mixed propellants being proposed as a solution to investigate this further.

The various assumptions applied when using the standard Hall thruster scaling laws have been demonstrated to have a large effect on the theoretical thruster performance, even more so when the effect of different propellants is considered. In particular the assumed neutral thermal velocity and also the widely applied Melikov-Morozov criterion are demonstrated to be overly simplistic, and further studies are required to adequately capture their effects on the design of an optimal thruster geometry. The investigation into the feasibility and challenges of gaseous and inert alternative propellants has been undertaken successfully, resulting in several areas identified as requiring further research to allow the increased ease of use and designing for alternative propellant Hall thrusters. The assumptions regarding the current assumptions of the neutral thermal velocity and its effects upon scaling and theoretical calculations of performance are outlined and highlighted as requiring additional work.

8. Future work

Due to the promise shown by nitrogen as a viable alternative to argon in small HET, further research into a HET designed for lighter propellant discharges should be manufactured and tested. This would allow for these two propellants to be more directly compared through further comprehensive tests. If nitrogen is indeed a viable alternative to argon, this could decrease the cost of large mass throughput testing by orders of magnitude. This work would also benefit from a comparative study with the differing erosion rates between xenon, argon, and nitrogen over similar total mass throughput, potentially allowing for on ground testing to use nitrogen for lifetime estimates with xenon.

Neon was not able to be operated continuously with the current set-up due to requiring a level of xenon to be present for any discharge to occur. This can be better explored in a future with a set up that allows for accurate mixing of the propellants allowing for accurate data to be collected. This mixed testing can be conducted for all propellants and could open the door for designing HET propellants for specific thrust and specific impulse levels for the same power and thruster geometry.

Declaration of competing interest

The authors declare that they have no known competing financial interests or personal relationships that could have appeared to influence the work reported in this paper.

Acknowledgement

This research did not receive any specific grant from funding agencies in the public, commercial, or not-for-profit sectors.

References

- [1] D. Selva, A. Golkar, O. Korobova, I.L.I. Cruz, P. Collopy, O.L. de Week, Distributed earth satellite systems: What is needed to move forward? *J. Aerosp. Inf. Syst.* 14 (8) (2017) 412–438.
- [2] R. Sandau, Status and trends of small satellite missions for Earth observation, *Acta Astronaut.* 66 (1–2) (2010) 1–12.
- [3] I. Levchenko, K. Bazaka, Y. Ding, Y. Raitses, S. Mazouffre, T. Henning, P.J. Klar, S. Shinohara, J. Schein, L. Garrigues, et al., Space micropropulsion systems for cubesats and small satellites: From proximate targets to furthermost frontiers, *Appl. Phys. Rev.* 5 (1) (2018) 011104.
- [4] R.W. Conversano, D.M. Goebel, R.R. Hofer, I.G. Mikellides, R.E. Wirz, Performance analysis of a low-power magnetically shielded Hall thruster: Experiments, *J. Propuls. Power* 33 (4) (2017) 975–983.
- [5] D.M. Goebel, I. Katz, Fundamentals of Electric Propulsion: Ion and Hall Thrusters, Vol. 1, John Wiley & Sons, 2008.
- [6] S. Mazouffre, Electric propulsion for satellites and spacecraft: Established technologies and novel approaches, *Plasma Sources. Sci. Technol.* 25 (3) (2016) 033002.
- [7] J.C. McDowell, The low earth orbit satellite population and impacts of the SpaceX starlink constellation, *Astrophys. J. Lett.* 892 (2) (2020) L36.
- [8] D. Lev, R.M. Myers, K.M. Lemmer, J. Kolbeck, H. Koizumi, K. Polzin, The technological and commercial expansion of electric propulsion, *Acta Astronaut.* 159 (2019) 213–227.
- [9] E.Y. Choueiri, A critical history of electric propulsion: The first 50 years (1906–1956), *J. Propuls. Power* 20 (2) (2004) 193–203.
- [10] M.J. Turner, Rocket and Spacecraft Propulsion: Principles, Practice and New Developments, Springer Science & Business Media, 2008.
- [11] S. Mazouffre, L. Grimaud, Characteristics and performances of a 100-W Hall thruster for microspacecraft, *IEEE Trans. Plasma Sci.* 46 (2) (2018) 330–337.
- [12] R.W. Conversano, D.M. Goebel, R.R. Hofer, T.S. Matlock, R.E. Wirz, Magnetically shielded miniature Hall thruster: Development and initial testing, in: The 33rd International Electric Propulsion Conference, the George Washington University, USA, The Electric Rocket Propulsion Society, 2013, p. 201.
- [13] Y. Daren, D. Yongjie, Z. Zhi, Improvement on the scaling theory of the stationary plasma thruster, *J. Propuls. Power* 21 (1) (2005) 139–143.
- [14] A.A. Shagaya, On scaling of Hall effect thrusters, *IEEE Trans. Plasma Sci.* 43 (1) (2013) 12–28.
- [15] K. Dannenmayer, S. Mazouffre, Elementary scaling relations for Hall effect thrusters, *J. Propuls. Power* 27 (1) (2011) 236–245.
- [16] S.-C. Hwang, R.D. Lein, D.A. Morgan, Noble gases, in: Kirk-Othmer Encyclopedia of Chemical Technology, vol. 17, American Cancer Society, 2005, pp. 343–383, <http://dx.doi.org/10.1002/0471238961.0701190508230114.a01.pub2>, Ch. Noble.
- [17] D.A. Herman, K.G. Unfried, Xenon acquisition strategies for high-power electric propulsion NASA missions, in: JANNAF SPS Subcommittee Meeting of the 62nd JANNAF Propulsion Meeting, JPM, Nashville TN, 2015.
- [18] M.L. McGuire, S.R. Oleson, L. Burke, S. McCarty, J.M. Newman, M. Martini, D. Smith, NASA GRC compass team conceptual point design and trades of a hybrid solar electric propulsion (SEP)/chemical propulsion human mars deep space transport (DST) vehicle, in: 2018 Aiaa SPACE and Astronautics Forum and Exposition, 2018, p. 5141.
- [19] C.P. Newman, D.C. Davis, R.J. Whitley, J.R. Guinn, M.S. Ryne, Stationkeeping, orbit determination, and attitude control for spacecraft in near rectilinear halo orbits, *Am. Astron. Soc.* (2018).
- [20] D.A. Herman, T. Gray, I. Johnson, S. Hussein, T. Winkelmann, Development and qualification status of the electric propulsion systems for the NASA PPE mission and gateway program, in: 37th International Electric Propulsion Conference, 2022, p. 465.
- [21] L.L. Su, A.R. Vazsonyi, B. Jorns, Performance of a 9-kW magnetically-shielded Hall thruster with krypton, in: AIAA Propulsion and Energy 2020 Forum, 2020, p. 3617.
- [22] J.A. Linnell, A.D. Gallimore, Efficiency analysis of a Hall thruster operating with krypton and xenon, *J. Propuls. Power* 22 (6) (2006) 1402–1418.
- [23] V. Tirilia, A. Demaire, A. Hallock, C. Ryan, The investigation of alternative solid propellants in Hall thrusters, in: Space Propulsion Conference 2020+1, 2021, p. 00061.
- [24] R. Dressler, Y.-H. Chiu, D. Levandier, Propellant alternatives for ion and Hall effect thrusters, in: 38th Aerospace Sciences Meeting and Exhibit, 2000, p. 602.
- [25] F. Paganucci, M. Saravia, M. Mininni, L. Bernazzani, A. Ceccarini, T. Boulzaguet, G. Pellegrini, C. Ducci, D. Pedrini, T. Andreussi, et al., Progress on the development of an iodine-fed Hall effect thruster, in: Atlanta: 35th International Electric Propulsion Conference, 2017, p. 418.
- [26] J. Szabo, M. Robin, V. Hruby, Bismuth vapor Hall effect thruster performance and plume experiments, in: Proceedings of the the 35th International Electric Propulsion Conference, 2017, pp. 2017–2025.
- [27] J.M. Makela, R.L. Washeleski, D.R. Massey, L.B. King, M.A. Hopkins, Development of a magnesium and zinc Hall-effect thruster, *J. Propuls. Power* 26 (5) (2010) 1029–1035.
- [28] J.A. Linnell, An Evaluation of Krypton Propellant in Hall Thrusters (Ph.D. thesis), University of Michigan, 2007.
- [29] M.R. Nakles, W.A. Hargus Jr., J.J. Delgado, R.L. Corey, A performance comparison of xenon and krypton propellant on an SPT-100 Hall thruster (preprint), Tech. Rep., AIR FORCE RESEARCH LAB EDWARDS AFB CA, 2011.
- [30] A. Bugrova, A. Bishaev, A. Desyatkov, M. Kozintseva, A. Lipatov, M. Dudeck, Experimental investigations of a krypton stationary plasma thruster, *Int. J. Aerosp. Eng.* 2013 (2013).
- [31] J. Kurzyna, M. Jakubczak, A. Szelecka, K. Dannenmayer, Performance tests of IPPLM's krypton Hall thruster, *Laser Particle Beams* 36 (1) (2018) 105.
- [32] C. Marrese, A. Gallimore, J. Haas, J. Foster, B. King, S. Kim, S. Khartov, An investigation of stationary plasma thruster performance with krypton propellant, in: 31st Joint Propulsion Conference and Exhibit, 1995, p. 2932.
- [33] B. Vincent, S. Tsikata, S. Mazouffre, Incoherent Thomson scattering measurements of electron properties in a conventional and magnetically-shielded Hall thruster, *Plasma Sources. Sci. Technol.* 29 (3) (2020) 035015.
- [34] R. Hofer, R. Lobbia, V. Chaplin, A. Lopez Ortega, I. Mikellides, J. Polk, H. Kamhawi, J. Frieman, W. Huang, P. Peterson, et al., Completing the development of the 12.5 kW Hall effect rocket with magnetic shielding (HERMeS), in: 36th International Electric Propulsion Conference, Vienna, Austria, September 15–20, 2019, Pasadena, CA: Jet Propulsion Laboratory, National Aeronautics and Space Administration, 2019, p. 193.
- [35] R.W. Conversano, R.B. Lobbia, T.V. Kerber, K.C. Tilley, D.M. Goebel, S.W. Reilly, Performance characterization of a low-power magnetically shielded Hall thruster with an internally-mounted hollow cathode, *Plasma Sources. Sci. Technol.* 28 (10) (2019) 105011.
- [36] T. Munro-O'Brien, C. Ryan, Design, manufacture and testing of a magnetically shielded krypton Hall effect thruster, in: Space Propulsion Conference 2020, 7th Edition of the Space Propulsion Conference, 3AF, 2021, p. 402.
- [37] L. Grimaud, S. Mazouffre, Performance comparison between standard and magnetically shielded 200 W Hall thrusters with BN-SiO₂ and graphite channel walls, *Vacuum* 155 (2018) 514–523.
- [38] L. Grimaud, S. Mazouffre, Conducting wall Hall thrusters in magnetic shielding and standard configurations, *J. Appl. Phys.* 122 (3) (2017) 033305.
- [39] E. Lee, Y. Kim, H. Lee, H. Kim, G. Doh, D. Lee, W. Choe, Scaling approach for sub-kilowatt Hall-effect thrusters, *J. Propuls. Power* 35 (6) (2019) 1073–1079.
- [40] K. Dannenmayer, S. Mazouffre, Sizing of Hall effect thrusters with input power and thrust level: An empirical approach, *J. Tech. Phys.* 3–4 (49) (2008) <http://dx.doi.org/10.48550/ARXIV.0810.3994>, URL <https://arxiv.org/abs/0810.3994>.
- [41] R. Conversano, Low-Power Magnetically Shielded Hall Thrusters (Ph.D. thesis), UCLA, 2015.
- [42] J.A. Linnell, A.D. Gallimore, Krypton performance optimization in high-voltage Hall thrusters, *J. Propuls. Power* 22 (4) (2006) 921–925.
- [43] D. Jacobson, D. Manzella, 50 Kw class krypton Hall thruster performance, in: 39th AIAA/ASME/SAE/ASEE Joint Propulsion Conference and Exhibit, 2003, p. 4550.
- [44] R.R. Hofer, D.M. Goebel, I.G. Mikellides, I. Katz, Magnetic shielding of a laboratory Hall thruster. II. Experiments, *J. Appl. Phys.* 115 (2014) <http://dx.doi.org/10.1063/1.4862314>.
- [45] K. Kwon, A Novel Numerical Analysis of Hall Effect Thruster and Its Application in Simultaneous Design of Thruster and Optimal Low-Thrust Trajectory (Ph.D. thesis), Georgia Institute of Technology, 2010.
- [46] N.Z. Warner, Theoretical and Experimental Investigation of Hall Thruster Miniaturization (Ph.D. thesis), Massachusetts Institute of Technology, 2007.
- [47] J. Szabo, M. Robin, S. Paintal, B. Pote, V. Hruby, High density Hall thruster propellant investigations, in: 48th AIAA/ASME/SAE/ASEE Joint Propulsion Conference & Exhibit, 2012, p. 3853.
- [48] K. de Grys, A. Mathers, B. Welander, V. Khayms, Demonstration of 10,400 hours of operation on 4.5 kw qualification model Hall thruster, in: 46th AIAA/ASME/SAE/ASEE Joint Propulsion Conference & Exhibit, 2010, p. 6698.
- [49] G.-C. Potiriviti, C. Rotaru, Hall effect thruster erosion mechanism and the thruster lifetime, in: 2014 International Conference on Applied and Theoretical Electricity, ICATE 2014-Proceedings, 2014, pp. 6972684–6972684.
- [50] I. Mikellides, I. Katz, R. Hofer, D. Goebel, K. de Grys, A. Mathers, Magnetic shielding of the acceleration channel walls in a long-life Hall thruster, in: 46th AIAA/ASME/SAE/ASEE Joint Propulsion Conference & Exhibit, 2010, p. 6942.
- [51] H. Tahara, K. Imanaka, S. Yuge, Effects of channel wall material on thrust performance and plasma characteristics of Hall-effect thrusters, *Vacuum* 80 (11–12) (2006) 1216–1222.
- [52] Y. Ding, H. Sun, W. Peng, Y. Xu, L. Wei, H. Li, P. Li, H. Su, D. Yu, Experimental test of 200 W Hall thruster with titanium wall, Japan. *J. Appl. Phys.* 56 (5) (2017) 050312.
- [53] N. Gascon, M. Dudeck, S. Barral, Wall material effects in stationary plasma thrusters. I. Parametric studies of an SPT-100, *Phys. Plasmas* 10 (10) (2003) 4123–4136.
- [54] T.L. Hardenburger, M. Ennis, U. by Staff, Nitrogen, in: Kirk-Othmer Encyclopedia of Chemical Technology, American Cancer Society, 2005, pp. 1–23, Ch. 16.
- [55] A. Crowe, J. McConkey, Dissociative ionization by electron impact. II. N+ and N++ from N₂, *J. Phys. B: Atom. Mol. Phys.* 6 (10) (1973) 2108.

- [56] L. Biagioni, M. Saverdi, M. Berti, U. Cesari, M. Andrenucci, Design and preliminary characterization of a 5 kW Hall thruster prototype, in: Proc. 28th IEPC, 2003, p. 228.
- [57] R. Rejoub, B. Lindsay, R. Stebbings, Determination of the absolute partial and total cross sections for electron-impact ionization of the rare gases, *Phys. Rev. A* 65 (4) (2002) 042713.
- [58] R.C. Wetzel, F.A. Baiocchi, T.R. Hayes, R.S. Freund, Absolute cross sections for electron-impact ionization of the rare-gas atoms by the fast-neutral-beam method, *Phys. Rev. A* 35 (2) (1987) 559.
- [59] D. Rapp, P. Englander-Golden, Total cross sections for ionization and attachment in gases by electron impact. I. Positive ionization, *J. Chem. Phys.* 43 (5) (1965) 1464–1479.
- [60] E. Krishnakumar, S. Srivastava, Cross sections for the production of N+ 2, N++ N2+ 2 and N2+ by electron impact on N2, *J. Phys. B: At. Mol. Opt. Phys.* 23 (11) (1990) 1893.
- [61] R.J. LeRoy, Spectroscopic reassignment and ground-state dissociation energy of molecular iodine, *J. Chem. Phys.* 52 (5) (1970) 2678–2682.
- [62] A.C. Hillier, Revolutionizing Space Propulsion Through the Characterization of Iodine as Fuel for Hall-Effect Thrusters (Master's thesis), Air Force Institute of Technology, Wright-Patterson Air Force Base, Ohio, 2011.
- [63] M. Moisan, J. Pelletier, Physics of Collisional Plasmas: Introduction to High-Frequency Discharges, Springer Science & Business Media, 2012.
- [64] J. Fisher, A. Wilson, D. King, S. Meyer, K. de Grys, L. Werthman, The development and qualification of a 4.5-kW Hall thruster propulsion system for GEO satellite applications—status update, in: 28th International Electric Propulsion Conference, Toulouse, France, 2003.
- [65] J.J. Szabo, B. Pote, R. Tedrake, S. Paintal, L. Byrne, V.J. Hruby, H. Kamhawi, T. Smith, High throughput 600 watt Hall effect thruster for space exploration, in: 52nd AIAA/SAE/ASEE Joint Propulsion Conference, 2016, p. 4830.
- [66] D. Jacobson, R. Jankovsky, Test results of a 200W class Hall thruster, in: 34th AIAA/ASME/SAE/ASEE Joint Propulsion Conference and Exhibit, 1998, p. 3792.
- [67] M.B. Belikov, O.A. Gorshkov, E.N. Dyshlyuk, A.S. Lovtsov, A.A. Shagayda, Development of low-power Hall thruster with lifetime up to 3000 hours, in: 30th Int. Electric Propulsion Conf., Florence, Italy, 2007, pp. 2007–129.
- [68] E. Rosati Azevedo, K. Jones-Tett, H. Larsen, S. Reeve, E. Longhi, J. Muñoz Tejeda, R. Moloney, A. Schwertheim, A. Knoll, Sizing and preliminary design of a 2-kW water propelled Hall effect thruster, in: Internaltional Electric Propulsion Conference, 2022, p. 317.
- [69] J.E. Polk, A. Pancotti, T. Haag, S. King, M. Walker, J. Blakely, J. Ziemer, Recommended Practices in Thrust Measurements, Tech. Rep., CALIFORNIA INST OF TECHNOLOGY PASADENA JET PROPULSION LAB, 2013.